Chapter 2

Mono lacunary silicotungstate (SiW_{11}) anchored to MCM-22:

Synthesis, Characterization and Esterification as well as Acetalization reactions

As mentioned in Part A Chapter 2, the mono lacunary silicotungstate (SiW_{11}) based catalysts have been utilized for various transformations. A literature survey shows, SiW_{11} supported on SiO_2 [1,2], mesoporous hybrid silica [3] and Metal Organic Framework [4] as well as metal doped SiW_{11} [5] have been explored mainly for oxidation reactions. However, the contribution for the development of anchored SiW_{11} based catalysts comes from Patel et. al group. They reported SiW_{11} anchored to zirconia, MCM-41 and Hβ and investigated for the catalytic acetalization, esterification and transesterification reactions for biodiesel synthesis [6–8]. Thus, the above literature survey depicts that very few reports are available on the development of anchored SiW_{11} and none of them reports their exploration in conversion of bioplatform molecules. Hence, in this direction, the successful exploration of MCM-22 as support for SiW_{12}, and its commendable catalytic activity for the transformation of bioplatform molecules, inspired us to develop another catalyst based on mono lacunary silicotungstate (SiW_{11}) and MCM-22. The focus was driven to understand the combination of SiW_{11} and MCM-22 via studying the effect of addenda atom on the similar catalytic applications.

In this chapter, a novel catalyst mono lacunary silicotungstate (SiW_{11}) anchored to MCM-22 was prepared by wet impregnation method and characterized in detail by various physicochemical techniques as mentioned in previous chapters. Similar catalytic applications, i.e., esterification and acetalization reactions of bioplatform molecules (Levulinic acid, succinic acid and glycerol) were carried out. The reaction conditions to obtain the maximum conversion of the substrate and to achieve selectivity of desired products were determined by a detailed optimization study. For this, several experiments with a varying mole ratio of reactants, catalyst amount, reaction temperature and time were screened. The sustainability, as well as the true heterogeneous nature of the catalyst, was studied by recycling experiments and characterization of regenerated catalyst. The activation energy for all the reactions was determined from kinetic experiments and the probable mechanism was proposed.

EXPERIMENTAL

Materials

All the chemicals of A. R. grade were utilized as received. Sodium tungstate dihydrate, sodium silicate, nitric acid (65%), acetone, levulinic acid, succinic acid, glycerol, furfural, n-butanol, ethanol, methanol, 2-propanol and dichloromethane were used as received from Merck. Zeolite MCM-22 was obtained commercially from BEE CHEMS (Kanpur, UP).

Synthesis of sodium salt of mono lacunary silicotungstate (SiW_{11})

The synthesis of SiW_{11} was carried out by the method discussed in Part A chapter-2.

Synthesis of catalyst, mono lacunary silicotungstate anchored to MCM-22 (SiW_{11}/MCM-22)

A series of a catalyst with 10 – 40% SiW_{11} anchored to MCM-22 was synthesized by the wet impregnation method. 1g of MCM-22 was suspended in an aqueous solution of SiW_{11} (0.1 g in10 mL – 0.4 g in 40 mL of distilled water) and the resulting suspension was dried at 100 ˚C till complete evaporation of water, followed by drying further for 10 h. The obtained solid material was treated with 0.1 N HCl solution to exchange the Na^+ ions of SiW_{11} into H^+ ions, followed by washing with water and drying. The obtained catalysts were designated as $(SiW_{11})_1$/MCM-22, $(SiW_{11})_2$/MCM-22, $(SiW_{11})_3$/MCM-22, and $(SiW_{11})_4$/MCM-22, respectively. A schematic representation of the procedure is shown in Scheme 1.

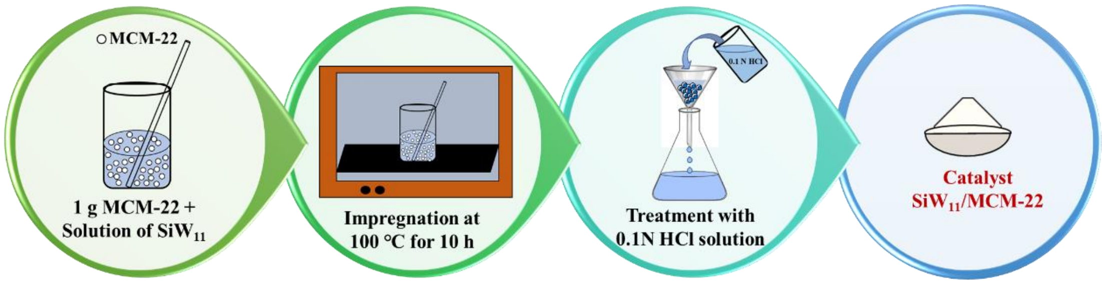

Scheme 1 Synthesis of SiW_{11}/MCM-22

Characterization

Characterization of SiW_{11}/MCM-22 was carried out by the same physicochemical techniques as mentioned in General Introduction [Page 41-46].

Catalytic activity

The esterification reaction of levulinic acid and succinic acid as well as the acetalization reaction of glycerol was carried out by following the same method as mentioned in General Introduction [Page 47-49].

RESULTS AND DISCUSSION

Characterization of SiW_{11}

Detailed characterization of SiW_{11} is mentioned in Part A Chapter 2.

Characterization of SiW_{11}/MCM-22

Acidity measurement

The acidic strength, as well as sites of a series of catalysts (10 - 40%) SiW_{11}/MCM-22 were determined by the potentiometric titration, are shown in Table 1 and the change obtained in the electrode potential as a function of mEq/g of n-butylamine is displayed in Figure 1. As observed from the results, with the % loading of SiW_{11}, the acidic strength and sites increase. This enhancement is due to the presence of Bronsted acidity in SiW_{11}, which is directly related to its amount. Notably, a gradual increase in the very strong and strong acid sites was observed for 10 and 20% loaded catalysts. Interestingly, an upsurge in the strong acid was evident for 30 and 40% loaded catalysts with increased their total acid sites instantaneously. This observation leads to the inference that SiW_{11} distributes inside the zeolitic support and increases its acidic strength. However, a minor difference in the acidic characteristics was observed between 30 and 40% loaded catalysts. This may be due to the blocking of sites or saturation of porous framework, similar to the trend observed in other catalysts. Thus, looking at the above observations, a 30% loading amount was found to be optimum.

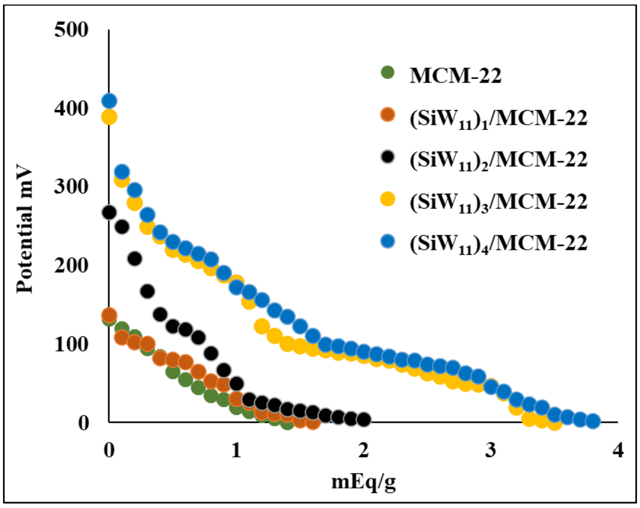

Figure 1 Potentiometric titration curves

Table 1 Acidity measurements of support and catalysts

Materials	Acidic strength (mV)	Types of acidic sites (mEq/g)		Total No. of acidic sites (mEq/g)
		Very strong	Strong	
MCM-22	132	0.2	1.2	1.4
$(SiW_{11})_1$/MCM-22	137	0.3	1.3	1.6
$(SiW_{11})_2$/MCM-22	268	0.8	1.2	2.0
$(SiW_{11})_3$/MCM-22	383	1.1	2.1	3.2
$(SiW_{11})_4$/MCM-22	402	1.2	2.3	3.5

BET surface area measurement

The textural properties of MCM-22 and catalysts are tabulated in Table 2. The BET surface area, pore diameter and pore volume of MCM-22 was found to decrease when the % loading of SiW_{11} increased. This is another indication of effective filling of SiW_{11} inside the pores of MCM-22. Here also, this trend is very well distinct for 10 – 30% loading amount. However, when the amount of SiW_{11} increased to 40%, a reverse trend for the pore diameter and volume was observed. Therefore, considering the combined observation of acidity measurements as well as BET surface area measurements, a 30% loading amount of SiW_{11} was found to be optimum and further characterization of only this catalyst was carried out. For simplicity, the catalyst was re-coded as SiW_{11}/MCM-22.

Table 2 Textural properties of support and catalysts

Materials	BET Surface area (m^2/g)	Pore diameter (Å)	Pore volume (cm^3/g)
MCM-22	344	102.4	0.79
$(SiW_{11})_1$/MCM-22	334	67.7	0.47
$(SiW_{11})_2$/MCM-22	328	64.6	0.44
$(SiW_{11})_3$/MCM-22	324	57.8	0.38
$(SiW_{11})_4$/MCM-22	320	61.3	0.4

The Nitrogen adsorption-desorption isotherms of MCM-22 and SiW_{11}/MCM-22 are shown in Figure 2. As shown in the previous chapter, MCM-22 exhibits a type IV isotherm with H4 hysteresis loop. A similar isotherm was obtained for SiW_{11}/MCM-22 with a rectangular-shaped trend where a sudden increase in the adsorption quantity occurs at very low P/Po, a characteristic of zeolites, having micro as well as mesopores in the framework [9]. It extends up to a higher value, forming a virtually horizontal plateau which is in good agreement with the characteristic zeolitic nature of materials [10]. However, the narrow hysteresis loop becomes narrow, indicating the effective filling inside pores of MCM-22.

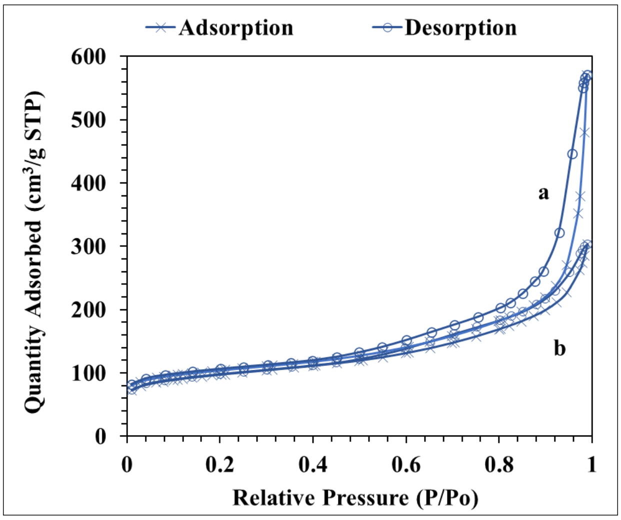

Figure 2 Nitrogen adsorption-desorption isotherms of a) MCM-22 and b) SiW_{11}/MCM-22

Elemental analysis

The effective loading of SiW_{11} was checked by performing an elemental analysis of SiW_{11}/MCM-22. The results are shown in Table 3 and Figure 3. The obtained wt% of tungsten (W) by EDS was found to be analogous to that of the theoretically calculated one, confirming successful loading of 30% SiW_{11}.

Table 3 Elemental analysis of catalyst

Material	Si (wt%)	O (wt%)	Al (wt%)	W (wt%)	
				By EDS	Theoretical
SiW_{11}/MCM-22	29.01	42.40	13.23	15.37	15.67

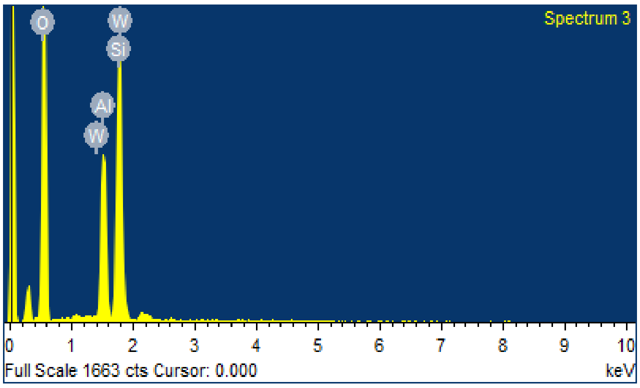

Figure 3 EDS elemental mapping of SiW_{11}/MCM-22

TGA

The TGA curves for MCM-22 and SiW_{11}/MCM-22 are shown in Figure 4. As explained earlier in the previous chapter, MCM-22 depicts weight loss in two steps. The first one, 4.7% weight loss is due to the desorption of adsorbed water up to 135 °C and the second one up to 200 °C is maybe because of the decomposition of the template, which was not completely removed [11]. A similar trend of weight loss was observed for catalyst, where the initial weight loss of about 5.71% was observed around 115 °C due to desorption of adsorbed water molecules. The final weight loss of about 2.0% up to 315 °C was obtained for the loss of crystalline water molecules present in SiW_{11}. Further, an absence of weight loss up to 600 °C, indicates higher thermal stability of the catalyst.

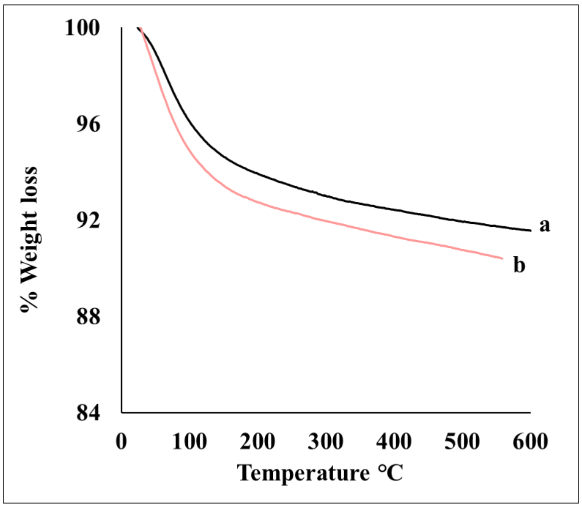

Figure 4 TGA curves of a) MCM-22 and b) SiW_{11}/nMCM-22

FT-IR

The FT-IR spectra of SiW_{11}, MCM-22 and SiW_{11}/MCM-22 are displayed in Figure 5. The characteristic bands of MCM-22 appear at 3441 cm^{-1}, 1226 cm^{-1}, 817 cm^{-1} and 455 cm^{-1}, corresponding to the O-H stretching of hydroxyl group, symmetric, asymmetric stretching vibrations of T-O-T bond, where T= Si or Al, and a stretching vibration for T-O, where the metal ion is bonded to four oxygen atoms, respectively [12]. The FT-IR spectra of SiW_{11}/MCM-22 exhibit all the above characteristic bands with an additional band at 810 cm^{-1} corresponding to the stretching frequency of W-O_c-W, present in SiW_{11} [13]. However, the bands of MCM-22 overlay the other characteristic bands of the keggin unit. Thus, the spectra show the presence of characteristic bands in the fingerprint region which indicates the intact structure of SiW_{11} as well as MCM-22 even after anchoring.

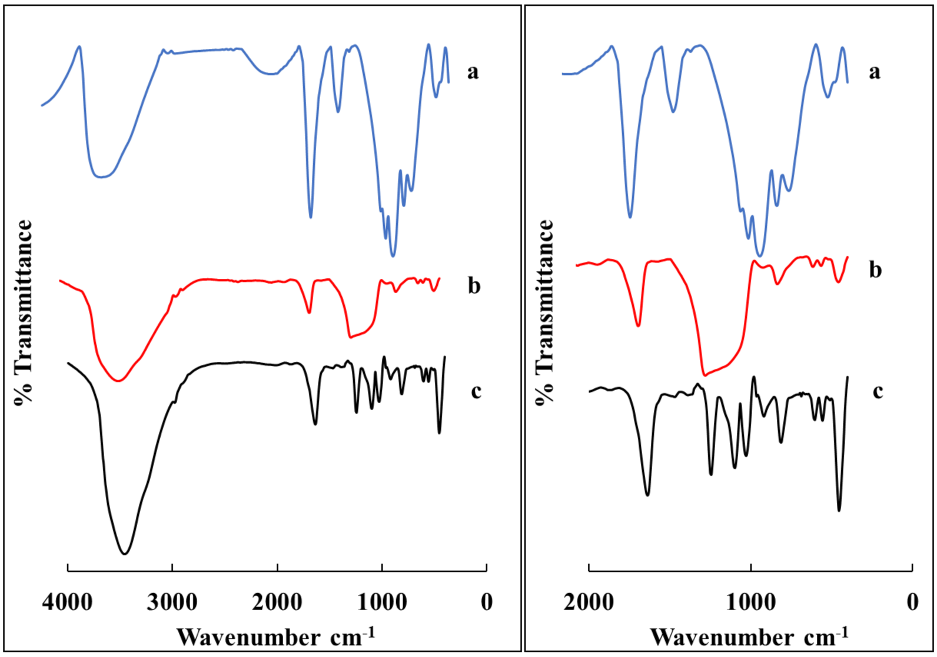

Figure 5 FT-IR spectra of a) SiW_{11} b) MCM-22 and c) SiW_{11}/MCM-22

Powder XRD

The powder XRD patterns of SiW_{11} (inset), MCM-22 and SiW_{11}/MCM-22 are shown in Figure 6. MCM-22 exhibits a well-resolved characteristic pattern in the range of 2θ 5 - 30° corresponding to the MWW framework of zeolitic structure

[14]. Similar peaks were observed in the pattern of SiW_{11}/MCM-22 with a little bit of decrease in the intensity due to the presence of SiW_{11}, indicating the unchanged crystalline framework of MCM-22 even after anchoring of SiW_{11}. Conversely, the crystalline peaks of SiW_{11} were not observed distinctly in the spectra which suggests uniform and fine dispersion of SiW_{11} species inside MCM-22.

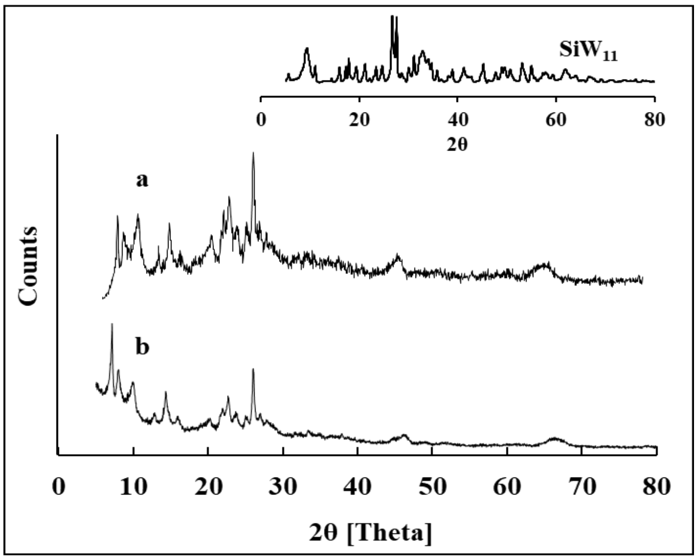

Figure 6 Powder XRD patterns of a) MCM-22, b) SiW_{11}/MCM-22 and SiW_{11} (Inset)

^{29}Si MAS NMR

The ^{29}Si MAS NMR spectra of MCM-22 and SiW_{11}/MCM-22 are shown in Figure 7. As mentioned in the previous chapter, MCM-22 show a distinct peak at -99.34 ppm, and a bunch of peaks from –102 to –118 ppm, corresponding to the Si nuclei associated with one Al unit and other Si (which are not surrounded by Al atoms), respectively [15,16]. While, in the spectra of SiW_{11}/MCM-22, an increase in the intensities of the above peaks was observed with a little bit of change in the chemical shift values due to an increase in the number of Si nuclei (which comes from SiW_{11}) in the vicinity. Thus, it validates the presence of hydrogen bonding between SiW_{11} and MCM-22. Moreover, an extra peak at -91.86 ppm was observed which is attributed to the Si nuclei of SiW_{11}. It shows the unchanged structure of the Keggin unit.

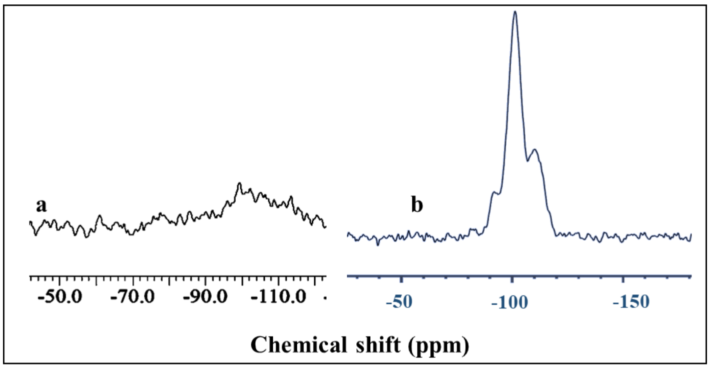

Figure 7 ^{29}Si MAS NMR of a) MCM-22 and b) SiW_{11}/MCM-22

TEM

The TEM image of MCM-22 (Figure 8a and b) exhibits uniform structure formed by the growth of flaky crystals. A distinct transparent pore networks with lamellar structure is observed [11]. For SiW_{11}/MCM-22 (Figure 8c and d), these pore networks appear to be opaque due to the filling of SiW_{11}, and no aggregation or change in the flaky crystal structure was seen. Also, it signifies uniform dispersion of active species inside the support which also supported by the XRD patterns.

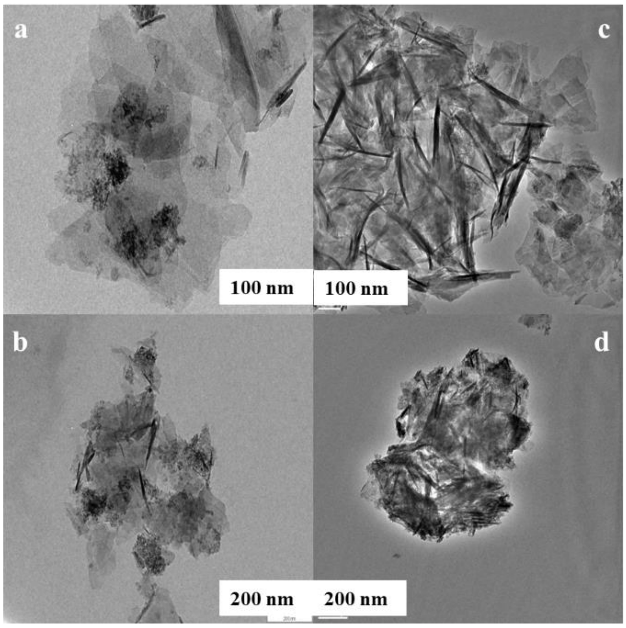

Figure 8 TEM images of a, b) MCM-22 and c, d) SiW_{11}/MCM-22

In brief, the increasing acidic character, as well as decreasing surface area in the support and series of catalysts, confirms the successful anchoring of SiW_{11} inside MCM-22. The thermal and FT-IR analysis validates higher stability at elevated temperature and unchanged structure of both the components, SiW_{11} as well as MCM-22, respectively. Powder XRD, and TEM analysis indicates the fine dispersion of actives species and support while the ^{29}Si MAS NMR corroborated the presence of hydrogen bonding between them.

Catalytic activity

Leaching test

The leaching of SiW_{12} from the hold of MCM-22 in SiW_{12}/MCM-22 was checked by the method given in General introduction [Page 46]. The absence of heteropoly blue colour indicates no leaching of SiW_{12} from MCM-22 and suggests the presence of chemical interaction between them as well as stability of the catalyst.

The catalytic activity of SiW_{11}/MCM-22 was studied to check its feasibility and the effect of the addenda atom for similar reactions of bioplatform molecules, as shown in previous chapters.

a) Esterification of levulinic acid with n-butanol

An in-depth study of all reaction parameters (% loading of SiW_{12}, mole ratio of levulinic acid to n-butanol, catalyst amount, reaction temperature and time) was carried out to obtain optimized reaction conditions for maximum conversion of levulinic acid and selectivity towards butyl levulinate.

Primarily, the influence of % loading amount of SiW_{11} in MCM-22 was studied and the obtained results for experiments with 10 - 40% loaded catalysts are portrayed in Figure 9a. Note that the initial feasibility of these catalysts was carried out in the optimized conditions obtained for SiW_{12}/MCM-22 (where time is 8 h), as there was only a difference of addenda atom. So, on increasing the %

loading of SiW_{11}, the reaction proceeds in a forward direction, giving a maximum conversion of levulinic acid as well as selectivity for ester in a 30% loading amount. This is in correlation with the results obtained for acidity and BET surface area measurements. Thus, also from a catalytic point of view 30% loading of SiW_{11} was found to be appropriate.

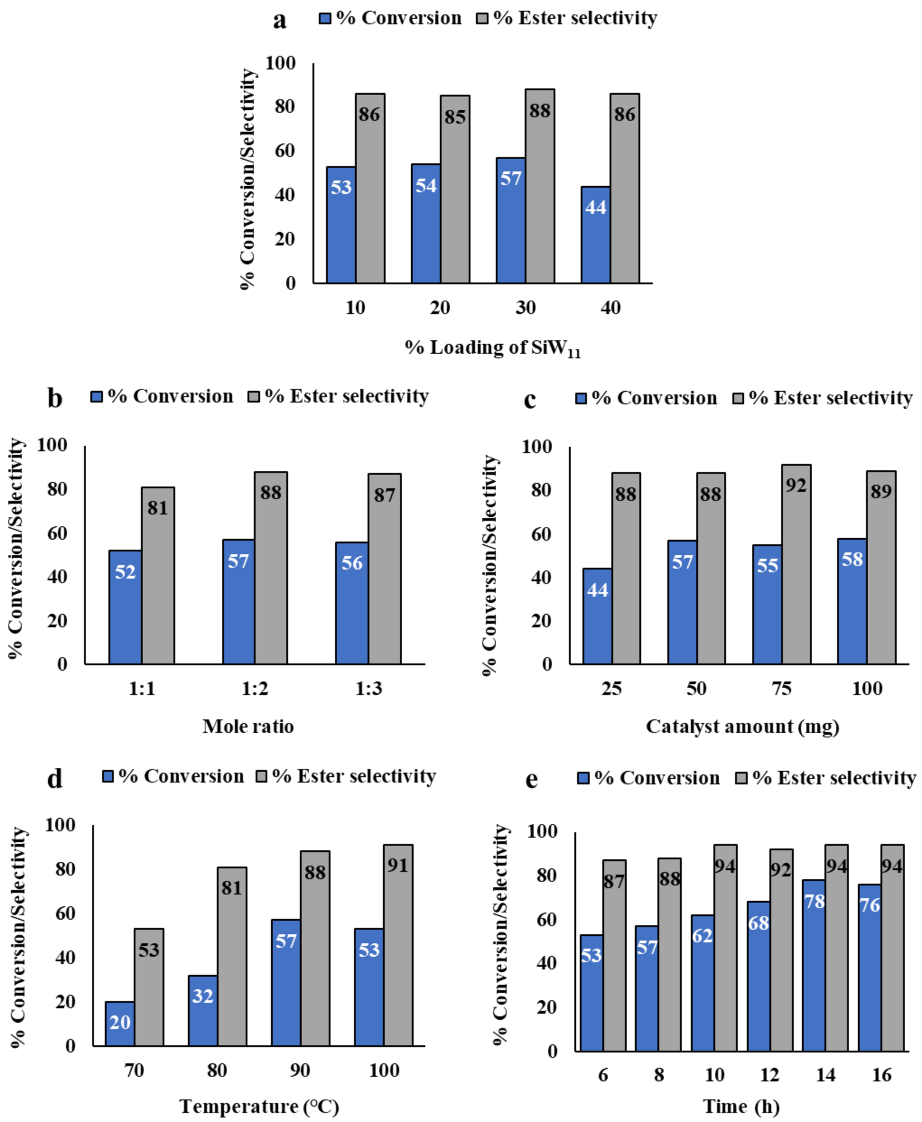

Figure 9 Reaction conditions. a) Effect of % loading of SiW_{11}. Mole ratio: 1:2; Catalyst amount: 50 mg; Temperature: 90 °C; Time: 8 h, b) Effect of mole ratio. Catalyst amount 50 mg; Temperature 90 °C; Time 8h, c) Effect of catalyst amount. Mole ratio 1:2; Temperature 90 °C; Time 8h, d) Effect of temperature. Mole ratio 1:2; Catalyst amount 50 mg; Time 8h. e) Effect of time. Mole ratio 1:2; Catalyst amount 50 mg; Temperature 90 °C.

In line, the second parameter, the mole ratio of levulinic acid to n-butanol was studied by varying it from 1:1 to 1:3 and the results are plotted in Figure 9b. As observed, the increase in the amount of alcohol has a positive effect on the conversion of levulinic acid as well as selectivity towards butyl levulinate. 52% conversion was attained in a 1:1 mole ratio, which hiked to 57% in 1:2. This may be attributed to the fact that as esterification is reversible, a little excess of alcohol shifts the equilibrium in a forward direction and thus we obtain better conversion in 1:2 ratio. However, on further increasing the ratio to 1:3, the conversion drops owing to dilution of the reaction mixture which demotes the rate of reaction. Therefore, a mole ratio of 1:2 was found to be optimum for this reaction with SiW_{11}/MCM-22.

To check the effect of catalyst amount, reactions were screened using 25 to 100 mg catalyst and the outcomes are depicted in Figure 9c. Certainly, an increase in the catalyst amount increases the availability of the active catalytic sites, which are responsible for the reaction. This fact is reflected in the results, where an increase in the catalyst amount from 25 mg to 50 mg, raised the conversion from 44% to 57% but no change in the selectivity of the ester was observed. However, on enhancing the amount to 75 and 100 mg, no major effect in the activity was noted. But, with more solid mass, the reaction mixture is difficult to stir as it becomes dense and slurry type. Considering the said aspects, 50 mg was optimized as the required catalyst amount.

The effect of temperature was studied by carrying out a reaction in a temperature range from 70 to 100 °C. From the obtained results (Figure 9d), expectedly, with the rise in temperature from 70 to 90 °C, the conversion of acid increases significantly from 20 to 57% along with the selectivity of ester from 53 to 88%. Nevertheless, at 100 °C, the conversion decreased by 4% which may be due to the evaporation of alcohol. Hence, as there was not much change in increasing the temperature by 10 °C, 90 °C was considered to be an appropriate temperature.

Lastly, the effect of time was studied and the reactions were carried out for 6 to 16 h. From the plot (Figure 9e), it is seen that with an increase in reaction time, the conversion increases linearly. Prolonging the reaction from 6 h to 14 h, the conversion increased from 53 to 78%. However, on increasing time to 16 h, the conversion decreased. This is mainly because with reaction time beyond the optimum, the concentration of product increases gradually which hampers the forward reaction. Therefore, the reaction time of 14 h was optimized.

From the above study with SiW_{11}/MCM-22, the optimized reaction conditions for maximum conversion of levulinic acid (78%) and selectivity of ester (94%) are mole ratio (levulinic acid: n-butanol) 1:2; catalyst amount 50 mg (active amount of SiW_{11} 11.54 mg), temperature 90 °C and time 14 h. The TON and TOF were found to be 2069 and 148 h^{-1} respectively.

b) Esterification of succinic acid with n-butanol

The catalytic activity of SiW_{11}/MCM-22 was also explored for the esterification of succinic acid with n-butanol and a detailed optimization study for achieving maximum conversion and selectivity of diester was carried out to find the suitable parameters.

To identify the appropriate % loading of SiW_{11}, a series of catalysts with 10 – 40% SiW_{11}/MCM-22 were screened. From the results (Figure 10a), it is observed that a gradual increase in the amount of SiW_{11} favours the conversion of succinic acid as well as diester formation. The observed pattern is similar to the expected trend which was also evident in previous catalysts. In 10% loading, lease conversion as well selectivity of diester was obtained, and in 30% loading, a maximum of 71% conversion with 39% selectivity of diester was achieved. On the contrary, increasing amount to 40%, the reaction does not progress and selectivity dropped slightly. As observed in the previous chapter, higher concentrations may lead to blocking of the sites and hence a less available space for reactants to activate. Thus, considering the best results, 30% loading of SiW_{11} was optimized.

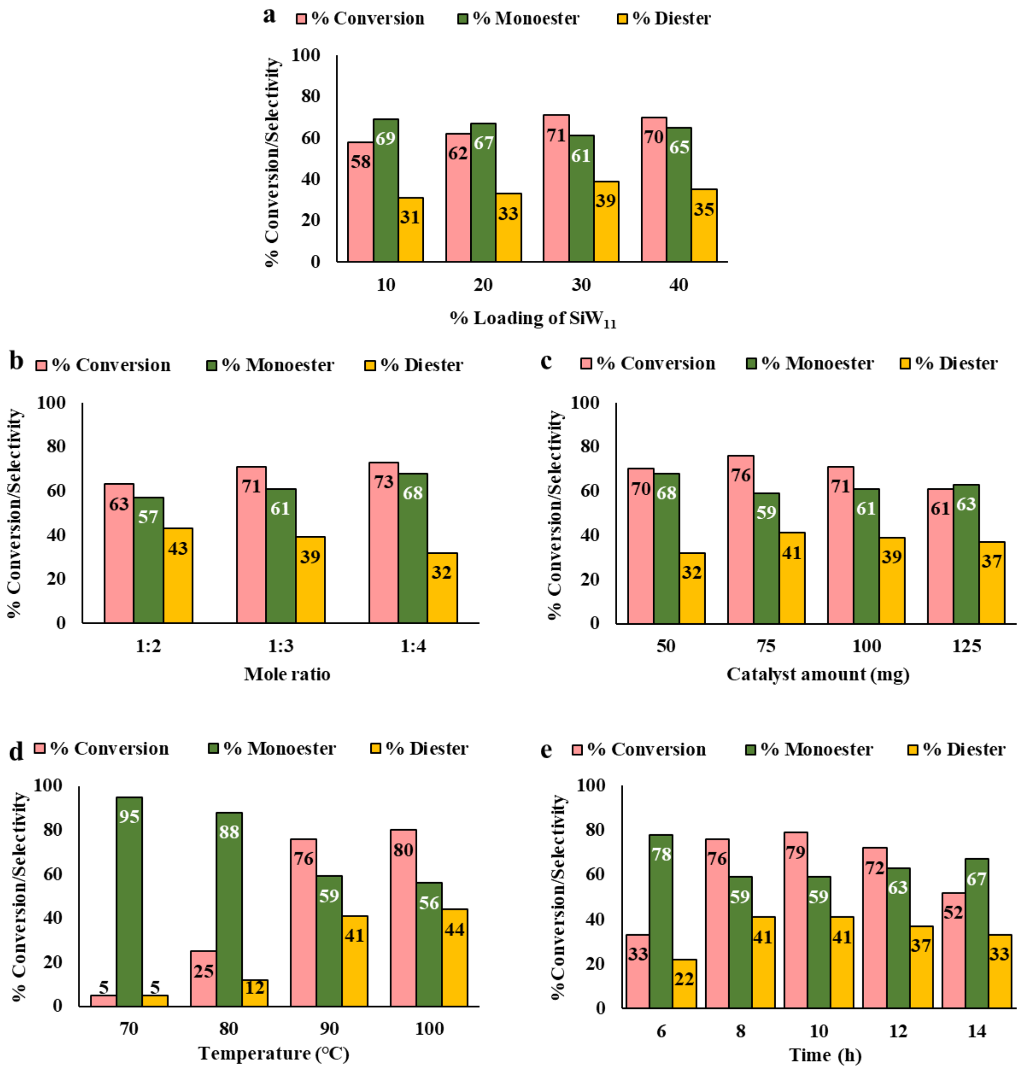

Figure 10 Reaction conditions. a) Effect of % loading of SiW_{11}. Mole ratio: 1:3; Catalyst amount: 100 mg; Temperature: 90 °C; Time: 8 h, b) Effect of mole ratio. Catalyst amount 100 mg; Temperature 90°C; Time 8h, c) Effect of catalyst amount. Mole ratio 1:3; Temperature 90°C; Time 8h, d) Effect of temperature. Mole ratio 1:3; Catalyst amount 75 mg; Time 8h e) Effect of time. Mole ratio 1:3; Catalyst amount 75 mg; Temperature 90°C.

The influence of the mole ratio was examined by keeping experiments in varying ratios and the results are shown in Figure 10b. From 1:2 to 1:4 the conversion of succinic acid increases from 63 to 73%. More concentration of alcohol assists the reaction to proceed in a forward direction. However, a reverse trend was observed for diester formation with an increasing ratio. This is because by increasing the alcohol concentration, dilution of the reaction mixture occurs, which in turn impedes the diesterification step. Also, it should be noted that no major augmentation in % conversion was observed when the ratio was increased from 1:3 to 1:4. Therefore, the 1:3 ratio was found to be optimum.

The effect of catalyst amounts from 50 to 125 mg was investigated and the obtained results are depicted in Figure 10c. As the catalyst amount increases, the available catalytic sites also increase and thus, from 50 to 75 mg the conversion of acid as well as selectivity towards diester increases. A maximum of 76% conversion with 41% selectivity of diester was obtained in 75mg catalyst. However, in 100 and 125 mg, the conversion dropped, because there is an increase in the mass density of the reaction mixture relative to that in lower catalyst amount. Thus, due to improper stirring, the reaction becomes sluggish in a higher catalyst amount. Taking into account the said aspects, 75 mg catalyst amount was found to be appropriate for this reaction.

Subsequently, the effect of the most vital reaction parameter for the esterification process, the reaction temperature was scrutinized. The obtained results (Figure 10d) reflect that temperature plays a major role in governing the reaction in a forward direction. At 70 °C, only 5% conversion of acid was observed, which hiked to 76% at 90 °C. This sudden change can be attributed to the easy transport of reactant molecules to the active catalytic sites as well as a massive increase in the collisions between them to convert into products. Additionally, elevated temperature favoured the diester formation. But there was no significant improvement in the results when the temperature was increased to 100 °C. So, 90 °C was fixed as an optimized temperature.

To check the effect of time, reactions were carried out for 6 to 14 h (Figure 10e). A sudden increase in the conversion of acid was observed when the reaction time was extended from 6 to 8 h. Only 33% conversion and 22% diester selectivity were attained in 6 h, but in 8 h, the conversion boosted to 76% with 41% diester selectivity. This suggests that in less reaction time, a smaller number of acid molecules gets activated and when the time is prolonged, sufficient reactant molecules get converted into products. After that, no significant change was observed. Hence, 8 h was considered to be the optimum reaction time.

The optimized reaction conditions for maximum conversion of succinic acid (76%) and selectivity of diester (41%) using SiW_{11}/MCM-22 are mole ratio of acid to alcohol 1:3, catalyst amount 75 mg (active amount of SiW_{11} 17.3 mg), temperature 90 °C and time 8 h. The TON and TOF were found to be 1343 and 168 h^{-1} respectively.

(c) Acetalization of glycerol with furfural

The catalytic efficiency of SiW_{11}/MCM-22 for acetalization of glycerol with furfural was evaluated. Its detailed optimization study was carried out by varying similar reaction parameters as mentioned previously, to determine the optimum reaction conditions for maximum conversion of glycerol and dioxane selectivity.

The initial viability of a series of catalysts with 10 - 40% loading of SiW_{11} was checked and the results are tabulated in Figure 11a. As observed in previous studies, with an increase in the % loading of SiW_{11}, the conversion of glycerol increases significantly. This progress in the reaction can be attributed to the increase in acid sites responsible for the activation of the carbonyl group of furfural. The trend is evident for 10 to 30 % loading. A maximum conversion of 54% with 69% dioxane selectivity was achieved in 30% loading, however, when the concentration of SiW_{11} increased to 40%, the conversion slightly drops with no change in the selectivity of dioxane. Therefore, considering the acidity as well as better feasibility for this reaction, 30% loading of SiW_{11} was optimized for further catalytic study.

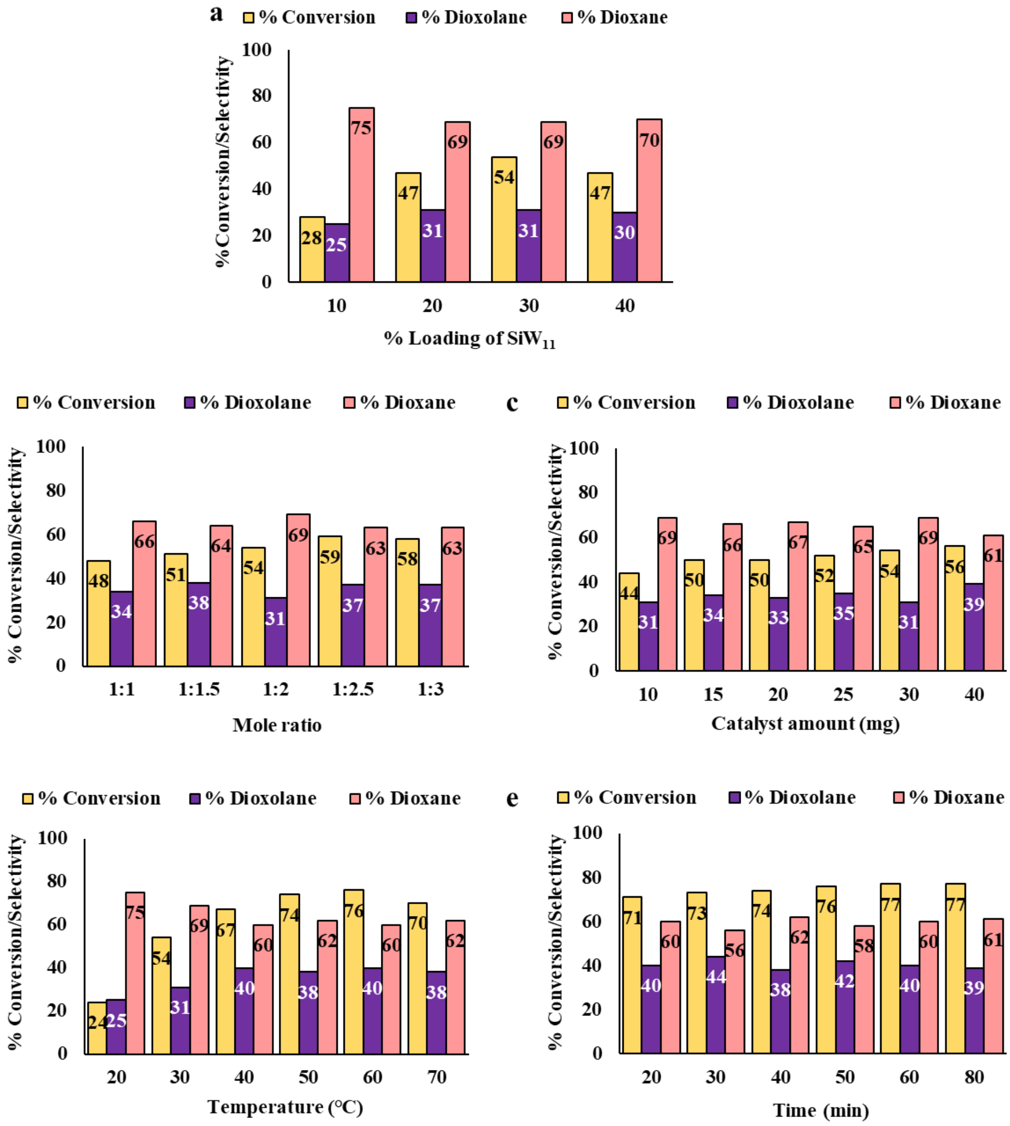

Figure 11 Reaction conditions. a) Effect of % loading of SiW_{11}. Mole ratio 1:2; Catalyst amount 30 mg; Temperature 30 °C; Time 40 min, b) Effect of mole ratio. Catalyst amount 30 mg; Temperature 30°C; Time 40 min, c) Effect of catalyst amount. Mole ratio 1:2; Temperature 30°C; Time 40 min, d) Effect of temperature. Mole ratio 1:2; Catalyst amount 30 mg; Time 40 min, e) Effect of time. Mole ratio 1:2; Catalyst amount 30 mg; Temperature 50°C.

The mole ratio of glycerol to furfural varied from 1:1 to 1:3 and the obtained results are plotted in Figure 11b. An upsurge in the mole ratio from 1:1 to 1:2 emphatically improves the conversion of glycerol. But no significant change was observed when the concentration of furfural is increased to 2.5 or 3 times i.e., 1:2.5 or 1:3 mole ratio. This may be due to the attainment of equilibrium. Hence, the 1:2 mole ratio was found to be appropriate for said reaction.

Following this, the effect of catalyst amount was investigated. The obtained results (Figure 11c) show that there is a gradual increment in the % conversion of glycerol with an increase in catalyst amount from 10 to 30 mg. A better conversion of glycerol (54%), as well as dioxane selectivity (69%), was achieved in 30 mg catalyst. In lower catalyst amounts, enough catalytic sites for the activation of furfural are not available and, in an amount, beyond 30 mg the density of the reaction mixture may affect the forward reaction due to improper stirring or slurry formation. Henceforth, 30 mg was found to be a suitable catalyst amount for carrying out this reaction.

Undoubtedly, in any reaction, temperature plays a major role in governing it in a forward direction. Therefore, the influence of temperature on the reaction was examined by carrying out experiments at 20 – 70 °C. As observed from the results (Figure 11d), with temperature the conversion rate of glycerol increases significantly, and a maximum of 76% conversion and 60% dioxane selectivity was obtained at 60 °C. Nevertheless, there was no major difference in the results of 50 and 60 °C. Also, at 70 °C, a minor decrease in the activity was observed. So, 50 °C was found to be the optimum temperature.

The influence of reaction time was scrutinized in a range from 20 to 80 min. steady growth in the conversion rate was noticed from the plot (Figure 11e) which indicates that the reaction time does not influence much the progress of the reaction. An appreciable conversion of 74% and the highest selectivity of dioxane (62%) were achieved in 40 min reaction time. Prolonging the reaction time after 40 min did not show any fruitful effect, accordingly 40 min was fixed as the optimum reaction time.

From the above study, the optimized reaction parameters for maximum conversion of glycerol (74%) and dioxane selectivity (62%) over SiW_{11}/MCM-22 are mole ratio 1:2, catalyst amount 30 mg (active amount of SiW_{11} 7.0 mg), temperature 50 °C, time 40 min. The TON and TOF of 3267 and 4900 h^{-1}, respectively were obtained.

All products were identified and confirmed with their respective standards using gas chromatography. The gas chromatographs of all three reactions are shown in Figure 12, Figure 13 and Figure 14.

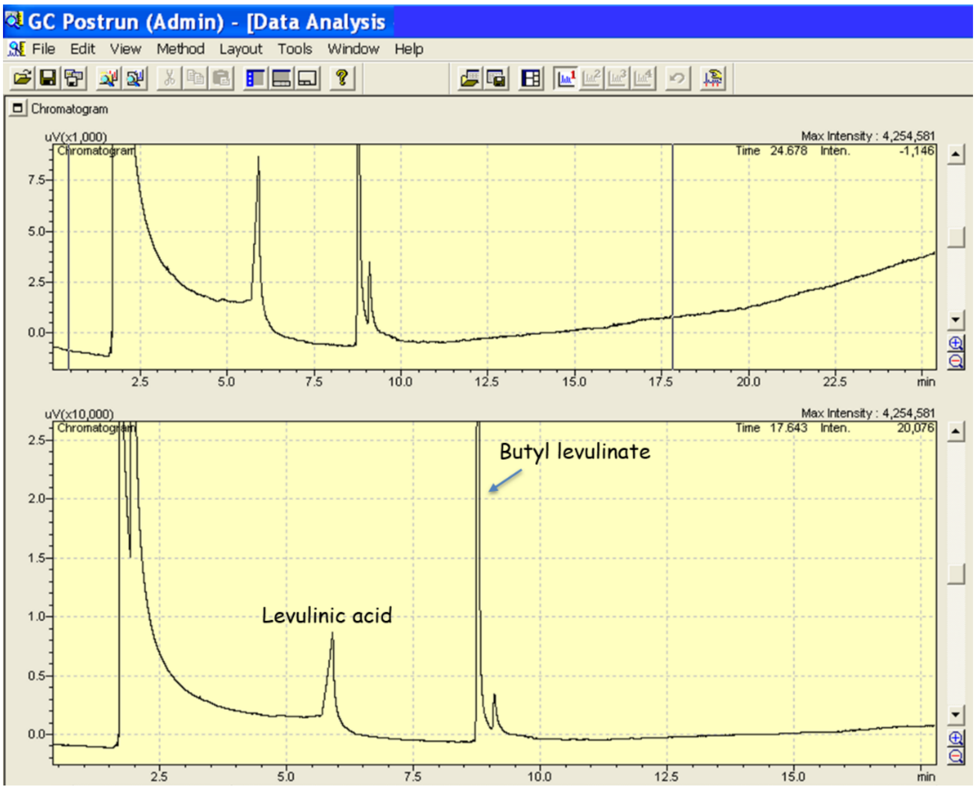

Figure 12 Gas chromatograph of levulinic acid esterification

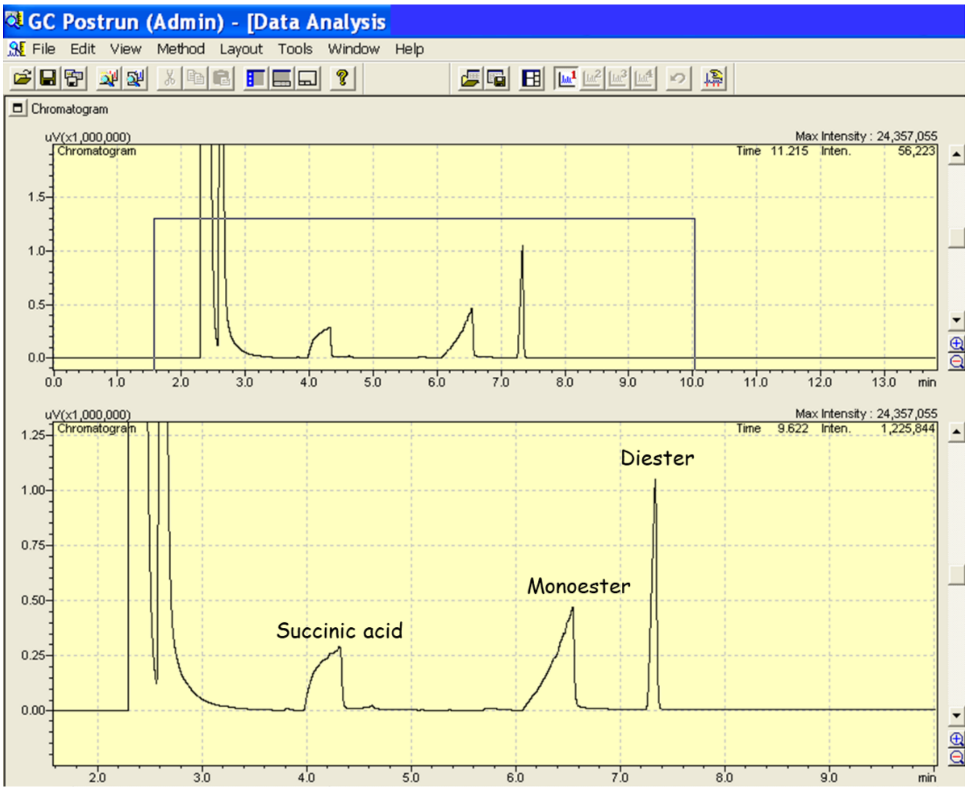

Figure 13 Gas chromatograph of succinic acid esterification

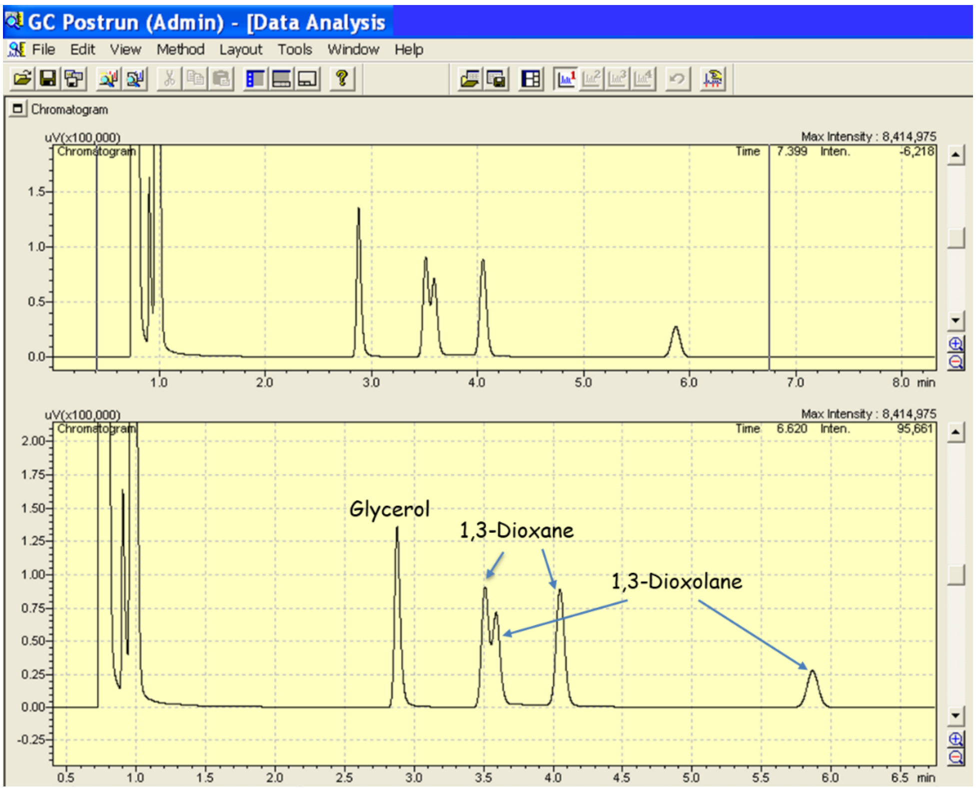

Figure 14 Gas chromatograph of glycerol acetalization

Control experiments

Control experiments with alone SiW_{11} and MCM-22 were examined for all reactions in their respective optimized conditions and the obtained results were compared with the catalyst, SiW_{11}/MCM-22. From the data given in Table 4, the activity of MCM-22 is less as compared to that of SiW_{11}, except for acetalization of glycerol. While higher conversion was obtained with alone SiW_{11}, as well as SiW11/MCM-22. This indicates the active catalytic sites, in the form of Bronsted acidity, are provided by SiW_{11}. Thus, SiW_{11} acts as active species and the support imparts successful heterogenization making it a truly heterogeneous catalyst.

Table 4 Control experiments for SiW_{11}/MCM-22

Materials	% Conversion/ %Selectivity of desired product		
	[a]Levulinic acid esterification	[b]Succinic acid esterification	[c]Glycerol acetalization
MCM-22	40/89	53/27	56/69
SiW_{11}	47/90	58/28	36/73
SiW_{11}/MCM-22	78/94	76/41	74/62

Reaction conditions mole ratio [a]1:2, [b]1:3, [c]1:2; catalyst amount MCM-22 [a]38.46 mg, [b] 57.7 mg, [c]23 mg; SiW_{11} [a]11.54 mg, [b]17.3 mg, [c]7.0 mg; SiW_{11}/MCM-22 [a]50 mg, [b]75 mg, [c]30 mg; temperature [a]90 °C, [b]90 °C, [c]50 °C; time [a]4 h, [b]8 h, [c]40 min.
*Selectivity of [a]Butyl levulinate, [b]Diester (Dibutyl succinate) and [c]1,3-dioxane

Regeneration and recycling studies

The regeneration of the catalyst, SiW_{11}/MCM-22, was carried out by the method reported in Part A Chapter 1 and employed for the consecutive cycles. The obtained results are shown in Figure 15.

For all reactions, the considerable catalytic activity of regenerated SiW_{11}/MCM-22 was achieved up to 3 or 4 cycles. In the case of esterification of levulinic acid, the catalyst showed consistent activity up to 2 cycles however, the conversion, as well as selectivity, dropped in the 3rd cycle. While for succinic acid esterification and glycerol acetalization, the conversion and selectivity of the desired product were persistent up to 3 cycles with a decrease in the 4th one. This decrease in the activity after can be attributed to the loss in catalyst amount during the regeneration step or there may be sticking of substrates. However, depending on the chemist's choice, one can also use it for more cycles until the catalyst is fully exploited. The repeated cycles showed the stability and sustainability of the catalyst and its true heterogeneous nature.

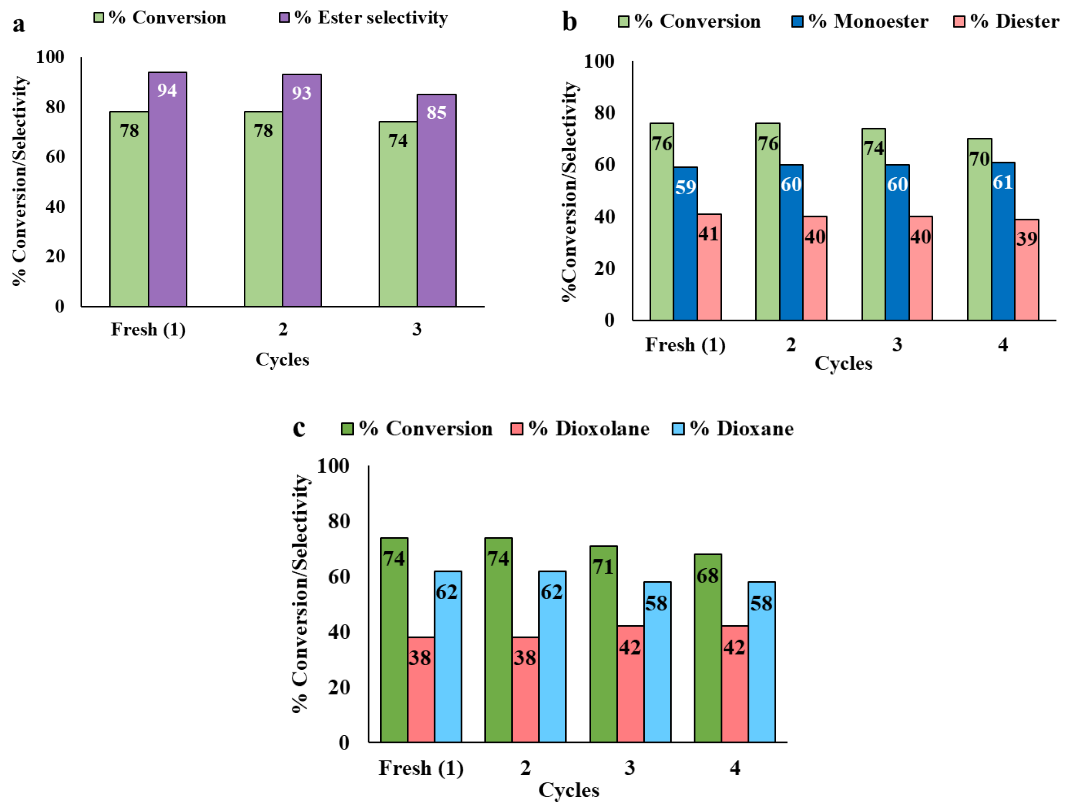

Figure 15 Recycling experiments for a) levulinic acid esterification, b) succinic acid esterification and c) glycerol acetalization

Characterization of regenerated catalyst

The regenerated SiW_{11}/MCM-22 was characterized by acidity measurements, BET surface area and FT-IR analysis. The acidic strength and total acidic sites of the regenerated catalyst were found to be in good agreement with that of the fresh one (Table 5), indicating its unchanged acidic nature. Also, identical N_2 adsorption-desorption isotherms of regenerated and fresh catalysts were obtained (Figure 16a and b), along with similar surface area, suggesting an intact structure of the catalyst. In the FT-IR spectra of regenerated catalyst, all the characteristic bands analogous to fresh catalyst were observed (Figure 16c). These observations signify the unaffected nature of the catalyst even after multiple cycles.

Table 5 Acidity measurements and BET surface area of fresh and regenerated catalyst

Catalyst	Acidic strength (mV)	Total acidic sites (mEq/g)	BET surface area (m^2/g)
Fresh	383	3.2	324
Regenerated	381	3.1	321

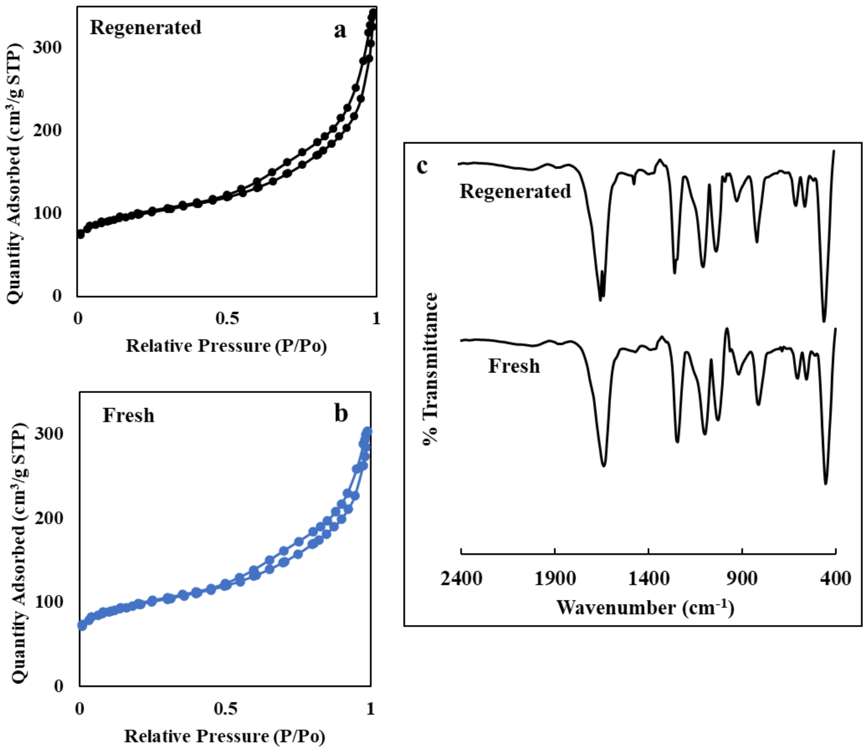

Figure 16 Nitrogen adsorption-desorption isotherms of a) regenerated and b) fresh catalyst and c) FT-IR spectra of regenerated and fresh catalyst

Activity of catalyst for esterification reactions under identical conditions

The results obtained from the experiments (Table 6) of the catalytic activity of SiW_{11}/MCM-22 for both esterification reactions indicates that appreciable conversion of levulinic acid (78%) as well as selectivity towards desired ester (94%) was achieved. However, only 28% conversion of succinic acid was observed with low selectivity of diester (24%). This observation directs that in longer reaction time (14 h), the catalyst manages to proceeds the reaction in forward direction for levulinic acid esterification. But when the succinic acid esterification was allowed to prolong for same time, the reaction may go in reverse direction, giving poor conversions. Hence, SiW_{11}/MCM-22 works better for levulinic acid esterification than for succinic acid.

Table 6 Esterification reactions under identical conditions

Conditions / Reactions	In optimized conditions of levulinic acid esterification*	
	% Conversion of acid	% Selectivity of desired ester
Levulinic acid esterification	78	94
Succinic acid esterification	28	24 (Diester)

*Reaction conditions mole ratio 1:2; catalyst amount 50 mg; temperature 90 °C; time 14 h

Kinetic study: Determination of activation energy

Similar to previous studies, kinetic experiments at different temperatures and time were carried out to determine the activation energy for all reactions over SiW_{11}/MCM-22.

a) Activation energy for esterification of levulinic acid with n-butanol

Esterification of levulinic acid with n-butanol in a 1:2 ratio at 90 °C was carried out in different time intervals (10, 12 and 14 h) and a graph of 1/(a-x) Vs Time was plotted Figure 17. The graph shows a linear relationship with respect to time, suggesting the second-order dependence of reaction.

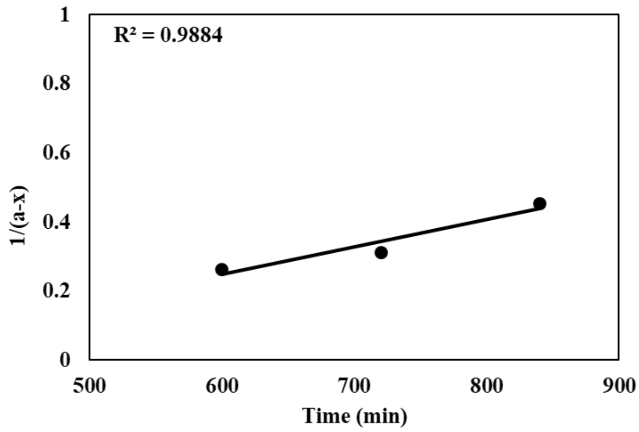

Figure 17 Plot of 1/(a-x) Vs Time for levulinic acid esterification

The rate constants at different temperatures (343 to 373 K) were calculated and obtained data is shown in Table 7. With the temperature rise, an increase in the rate constants was observed. Considering these values, a graph of ln *k* Vs 1/T was plotted and from the slope of the graph Figure 18, using the Arrhenius equation, the activation energy was calculated and found to be 49 kJ/mol.

Table 7 Rate constants (k M^{-1} min^{-1}) and activation energy (Ea)

Temperature (K)	Rate constant k (M^{-1} min^{-1})	Activation energy Ea (kJ/mol)
343	2.0×10^{-4}	
353	3.0×10^{-4}	49
363	5.0×10^{-4}	
373	7.8×10^{-4}	

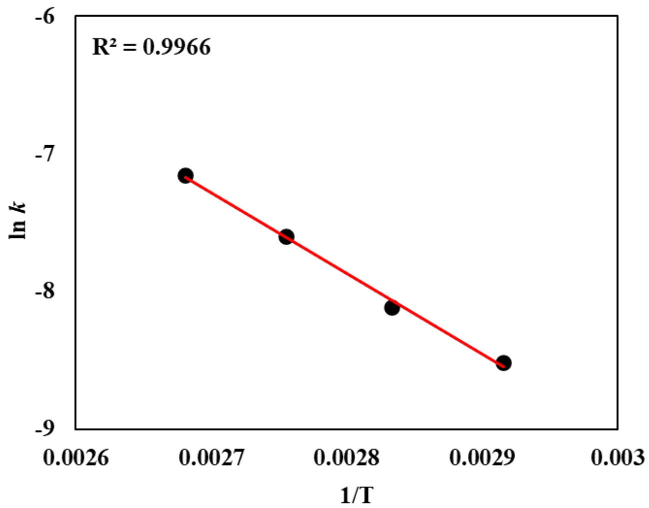

Figure 18 plot of ln k Vs 1/T for levulinic acid esterification

b) Activation energy for esterification of succinic acid with n-butanol

Analogous to previous studies, the kinetic experiments for the esterification of succinic acid and n-butanol using SiW_{11}/MCM-22 were carried out in 1:3 molar ratio at 90 °C, for different time intervals (6, 8 and 10 h) and a graph of 1/(a-x) Vs Time was plotted (Figure 19). The graph shows a linear relationship with respect to time and follows the second-order dependence of the reaction.

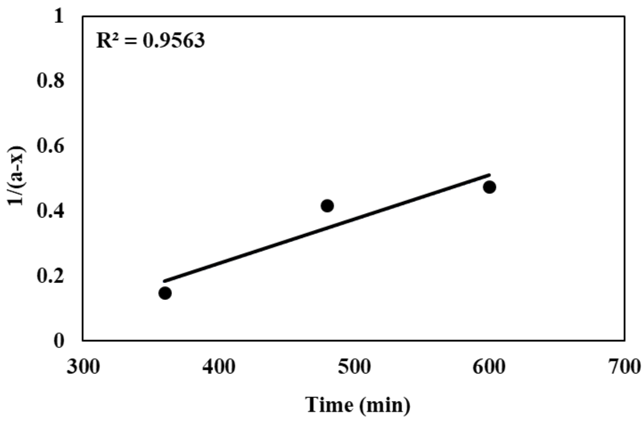

Figure 19 Plot of 1/(a-x) Vs Time for succinic acid esterification

The rate constants at different temperatures were determined and the obtained results are mentioned in Table 8. Using the values of rate constants, the graph of ln k Vs 1/T was plotted (Figure 20). The activation energy for succinic acid esterification over SiW_{11}/MCM-22 was determined from the slope of the graph by using the Arrhenius equation and found to be 82 kJ/mol.

Table 8 Rate constants (k M^{-1} min^{-1}) and activation energy (Ea)

Temperature (K)	Rate constant k (M^{-1} min^{-1})	Activation energy Ea (kJ/mol)
343	2.0×10^{-4}	82
353	3.0×10^{-4}	
363	7.0×10^{-4}	
373	2.0×10^{-3}	

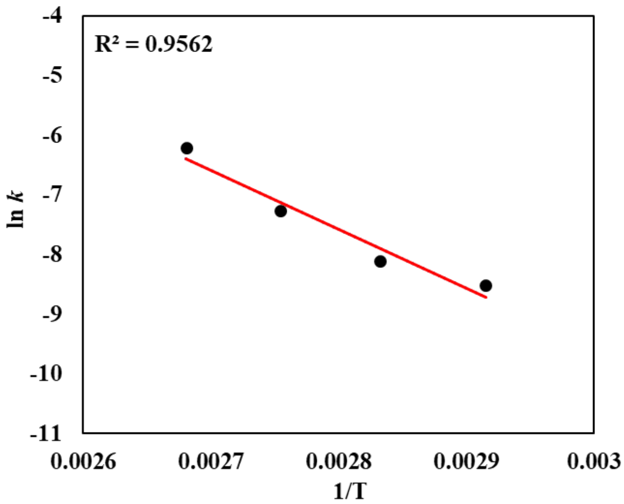

Figure 20 Plot of ln k Vs 1/T for esterification of succinic acid.

c) Activation energy for acetalization of glycerol with furfural

Acetalization of glycerol with furfural was carried out in a 1:2 mole ratio at 50 °C in different time intervals and from the obtained results, the graph of 1/(a-x) Vs Time was plotted (Figure 21). As observed, the graph shows a liner relationship with respect to time, indicating that reaction follows second-order dependence.

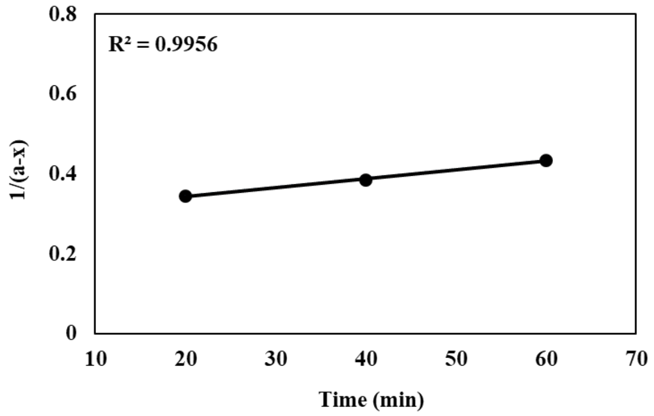

Figure 21 Plot of 1/(a-x) Vs Time for glycerol acetalization

The rate constants were determined at different temperatures (303 to 333 K) (Table 9) and from that graph ln *k* Vs 1/T was plotted Figure 22. The activation energy was determined from the slope of the graph using the Arrhenius equation and found to be 67 kJ/mol.

Table 9 Rate constants (k M^{-1} min^{-1}) and activation energy (Ea)

Temperature (K)	Rate constant k (M^{-1} min^{-1})	Activation energy Ea (kJ/mol)
303	4.9×10^{-4}	67
313	1.2×10^{-3}	
323	2.2×10^{-3}	
333	5.7×10^{-3}	

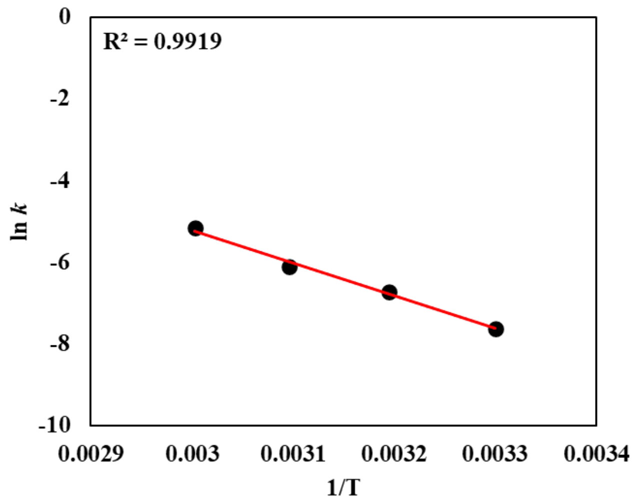

Figure 22 Plot of ln *k* Vs 1/T for glycerol acetalization

As a general observation, equivalent to previous studies with a different catalyst, here also, the activation energy for all reactions was beyond 25 kJ/mol. This intimates that with SiW_{11}/MCM-22 also, all the reactions follow a kinetic regime and are governed truly by a chemical step, the reactions are not limited to a diffusion regime [17]. Moreover, the catalyst at its maximum efficiency lowers the activation energy for levulinic acid esterification as compared to succinic acid esterification.

The trend in activation energies is similar to that of the previous catalysts. However, it should be noted that the activation energy obtained for all the reactions with the present catalyst is higher as compared to that with the previous three catalysts. The combination of SiW_{11} and MCM-22 only moderately lowers the activation energy as it possesses a less acidic character relative to other catalysts.

Plausible mechanism

For all three catalytic transformations using SiW_{11}/MCM-22, we are expecting the same mechanism as explained in Part B Chapter 1 for SiW_{12}/MCM-22. Hence detailed explanation is not included here.

CONCLUSION

- Successful synthesis and detailed characterization of a novel heterogeneous catalyst comprising mono lacunary silicotungstate and MCM-22 was carried out for the first time.
- A concordant approach of SiW_{11} and MCM-22 towards the catalytic esterification as well as acetalization reactions is reflected in gaining good conversions (≥ 74%) as well as selectivity towards desired products.
- At ambient temperatures, the activation energy was found to be 49 kJ/mol for levulinic acid esterification, 82 kJ/mol for succinic acid esterification and 67 kJ/mol for glycerol acetalization.

REFERENCES

1. D. Li, Y. Guo, C. Hu, L. Mao, and E. Wang, Appl Catal A Gen 235, 11 (2002).
2. Y. Guo, Y. Yang, C. Hu, C. Guo, E. Wang, Y. Zou, and S. Feng, J Mater Chem 12, 3046 (2002).
3. X. Luo and C. Yang, Phys Chem Chem Phys 13, 7892 (2011).
4. C. M. Granadeiro, A. D. S. Barbosa, P. Silva, F. A. A. Paz, V. K. Saini, J. Pires, B. de Castro, S. S. Balula, and L. Cunha-Silva, Appl Catal A Gen 453, 316 (2013).
5. X. Dong, C. Yu, D. Wang, Y. Zhang, P. Wu, H. Hu, and G. Xue, Mater Res Bull 85, 152 (2017).
6. S. Pathan and A. Patel, J Coord Chem 63, 4041 (2010).
7. A. Patel and N. Narkhede, Catal Sci Technol 3, 3317 (2013).
8. N. Narkhede and A. Patel, RSC Adv 4, 64379 (2014).
9. M. Thommes, K. Kaneko, A. v Neimark, J. P. Olivier, F. Rodriguez-Reinoso, J. Rouquerol, and K. S. W. Sing, Pure Appl Chem 87, 1051 (2015).
10. C. Delitala, M. D. Alba, A. I. Becerro, D. Delpiano, D. Meloni, E. Musu, and I. Ferino, Microporous Mesoporous Mater 118, 1 (2009).
11. Y. Cheng, X. Y. Su, and M. Lu, Adv Mat Res 197–198, 1587 (2011).
12. M. C. Lonare, S. N. Gaikwad, C. Lonare, R. G. Pala, S. Siva, and P. Kapse, IAETSD J Adv Res Appl Sci 5, 192 (2018).
13. T. Okuhara, N. Mizuno, and M. Misono, in edited by D. D. Eley, W. O. Haag, and B. B. T.-A. in C. Gates (Academic Press, 1996), pp. 113–252.
14. E. Xing, Y. Shi, W. Xie, F. Zhang, X. Mu, and X. Shu, RSC Adv 5, 8514 (2015).
15. W. Kolodziejski, C. Zicovich-Wilson, C. Corell, J. Perez-Pariente, and A. Corma, J Phys Chem 99, 7002 (1995).
16. A. L. Santos Marques, J. L. Fontes Monteiro, and H. O. Pastore, Microporous Mesoporous Mater 32, 131 (1999).
17. G. C. (Geoffrey C. Bond, Heterogeneous Catalysis : Principles and Applications / G.C. Bond (Clarendon Press, Oxford [Oxfordshire] ; New York, 1987).